arXiv:1511.07227v1 [astro-ph.GA] 23 Nov 2015

accepted by ApJ Letters

Molecular Gas and Star Formation in the Cartwheel

James L. Higdon[1], Sarah J. U. Higdon[1], Sergio Martín Ruiz[2], and Richard J. Rand[3]

ABSTRACT

Atacama Large Millimeter/submillimeter Array (ALMA) ^{12}CO(J=1-0) observations are used to study the cold molecular ISM of the Cartwheel ring galaxy and its relation to HI and massive star formation (SF). CO moment maps find $(2.69 \pm 0.05) \times 10^9$ M$_\odot$ of H_2 associated with the inner ring (72%) and nucleus (28%) for a Galactic $I_{\rm CO}$-to-$N_{\rm H_2}$ conversion factor ($\alpha_{\rm CO}$). The spokes and disk are not detected. Analysis of the inner ring's CO kinematics show it to be expanding ($V_{\rm exp} = 68.9 \pm 4.9$ km s^{-1}) implying an ≈ 70 Myr age. Stack averaging reveals CO emission in the starburst outer ring for the first time, but only where HI surface density ($\Sigma_{\rm HI}$) is high, representing $M_{\rm H_2} = (7.5 \pm 0.8) \times 10^8$ M$_\odot$ for a metallicity appropriate $\alpha_{\rm CO}$, giving small $\Sigma_{\rm H_2}$ (3.7 M$_\odot$ pc^{-2}), molecular fraction ($f_{\rm mol} = 0.10$), and H_2 depletion timescales ($\tau_{\rm mol} \approx 50 - 600$ Myr). Elsewhere in the outer ring $\Sigma_{\rm H_2} \lesssim 2$ M$_\odot$ pc^{-2}, $f_{\rm mol} \lesssim 0.1$ and $\tau_{\rm mol} \lesssim 140 - 540$ Myr (all 3σ). The inner ring and nucleus are H_2-dominated and are consistent with local spiral SF laws. $\Sigma_{\rm SFR}$ in the outer ring appears independent of $\Sigma_{\rm H_2}$, $\Sigma_{\rm HI}$ or $\Sigma_{\rm HI+H_2}$. The ISM's long confinement in the robustly star forming rings of the Cartwheel and AM0644-741 may result in either a large diffuse H_2 component or an abundance of CO-faint low column density molecular clouds. The H_2 content of evolved starburst rings may therefore be substantially larger. Due to its lower $\Sigma_{\rm SFR}$ and age the Cartwheel's inner ring has yet to reach this state. Alternately, the outer ring may trigger efficient SF in an HI-dominated ISM.

Subject headings: galaxies: individual(Cartwheel) — galaxies: interactions — galaxies: ISM — galaxies: starburst

[1]Department of Physics, Georgia Southern University, Statesboro, GA 30460-8031, USA

[2]Joint ALMA Office, Alonso de Coŕdova 3107, Vitacura, Casilla 19001, Santiogo 19, Chile

[3]Department of Physics and Astronomy, University of New Mexico, Albuquerque, NM 87131, USA

1. Introduction

Gravitational interactions play a fundamental role in galaxy evolution, from their assembly at high-z (White & Rees 1978; Jogee et al. 2009) to much of their subsequent chemical and luminosity evolution (Smail et al. 1997; Tacconi et al. 2008). Detailed studies of local interacting galaxies can provide important insights into these processes, particularly if the dynamical history can be reconstructed to allow detailed modeling. Ring galaxies, created in the passage of a companion through a spiral's disk, provide excellent examples. The interaction generates one or more outwardly traveling orbit-crowded rings that "snowplow" the disk's ISM as they propagate (Lynds & Toomre 1977; Struck & Higdon 1993; Mapelli et al. 2008) and trigger star formation (SF) via large-scale gravitational instabilities (Higdon 1996; Higdon, Higdon & Rand 2011, hereafter HHR). The rings host high and sustained SF throughout their $100 - 400$ Myr lifetimes as evidenced by numerical studies (see Fig. 12 in Mihos & Hernquist (1994) and Fig. 9 in Mapelli & Mayer (2012)) and observations of large optical/near-infrared radial color gradients from aging post-starburst clusters left in the ring's wake (e.g., Marcum, Appleton & Higdon 1993; Appleton et al. 1996; Romano, Mayya & Vorobyov 2008).

The ISM's long confinement in the rings provides a unique environment for studying the effects of massive stars on its state. AM0644-741's starburst ring, for example, appears to possess a remarkably low $M_{\rm H_2}$, molecular fraction ($f_{\rm mol} = M_{\rm H_2}/(M_{\rm HI} + M_{\rm H_2})$) and mean gas volume density ($n_{\rm H}$) despite conditions favoring an H_2-dominated ISM, along with a peculiar SF law in which $\Sigma_{\rm HI}$ but not $\Sigma_{\rm H_2}$ is correlated with $\Sigma_{\rm SFR}$ (HHR), i.e., a complete reversal of the situation in ordinary spirals, e.g., Kennicutt et al. (2007; K07), Bigiel et al. (2008; B08), Schruba et al. (2011; S11), and Leroy et al. (2013; L13). Is AM0644-741 unique or is its ISM characteristic of other large and robustly star forming ring galaxies? In this *Letter* we investigate the Cartwheel (Fig. 1), a similarly large (45 kpc), evolved (age $\approx R_{\rm ring}/V_{\rm exp} = 440$ Myr), and gas rich ($\rm M_{HI} = 2.9 \times 10^{10}\ M_\odot$) ring galaxy with comparable SFR (Higdon 1995, 1996) and - unique among ring galaxies - a small second ring. We combine deep ^{12}CO(J=1-0) observations with the Atacama Large Millimeter/submillimeter Array (ALMA) with optical, infrared and radio data from other telescopes. The molecular content of this galaxy has been a long-standing puzzle (Horellou et al. 1995, 1998; Higdon 1996). ALMA's revolutionary capabilities make it possible to examine the Cartwheel's molecular and atomic ISM and young stellar populations on comparable physical scales, allowing direct comparisons with local spirals.

2. Observations and Analysis

The Cartwheel was mosaiced with ALMA using 7-array pointings on 2013 December 24 (2012.1.00720.S) for uniform sensitivity to ^{12}CO(J=1-0) emission. The correlator provided a 468.8 MHz (1256 km s^{-1}) total bandwidth with 244.2 kHz (0.65 km s^{-1}) channels centered on the redshifted 115.2712 GHz line. Antenna gains and bandpass were calibrated using J0026-3512 while observations of Uranus set the absolute flux scale. CASA 4.2.1 was used for reduction (McMullin et al. 2007). A *natural*-weighted image cube consisting of 600 channels separated by 2.0 km s^{-1} was created and deconvolved using *imager*, giving a $2.43'' \times 1.50''$ (1.47×0.91 kpc) synthesized beam and a 1.39 mJy beam^{-1} rms. Integrated line flux (moment-0) and flux-weighted radial velocity (moment-1) maps are shown in Figs. 1 & 2. $M_{\rm H_2}$ is derived by multiplying the CO line luminosity ($L'_{\rm CO}$)

$$\mathrm{L'_{CO}} = \left(\frac{\mathrm{c^2}}{\mathrm{2k_B}}\right)\left(\frac{\mathrm{S_{CO}\Delta v}}{\mathrm{Jy\ km\ s^{-1}}}\right)\nu_{\rm obs}^{-2}\mathrm{D_L^2}(1+\mathrm{z})^{-3} \quad (1)$$

(Solomon & Vanden Bout 2005) by the appropriate $I_{\rm CO}$-to-$N_{\rm H_2}$ conversion factor: $\alpha_{\rm CO}$. All surface densities and masses are scaled by 1.36 to account for helium.

We also utilize long-slit optical spectra of both rings from the Mt. Stromlo & Siding Springs Observatory 2.3m telescope's double-beam spectrograph, a calibrated Hα emission-line image from the Canada France Hawaii Telescope, a MIPS 24 μm image, and Very Large Array integrated HI and velocity maps (Higdon 1996).

Hα and 24 μm emission is combined to derive internal extinction using

$$\mathrm{A_{H\alpha}} = 2.5\ \log\left(1\ +\ 0.038\frac{\nu \mathrm{L}_\nu(24\ \mu\mathrm{m})}{\mathrm{L_{H\alpha}}}\right) \quad (2)$$

(K07), where $L_\nu(24\ \mu m)$ and $L_{\rm H\alpha}$ are measured within identical $12''$ apertures. We find $A_{\rm H\alpha} = 0.4 - 1.4$ around the outer ring (consistent with Fosbury & Hawarden (1977)'s optical spectroscopy) and 1.9 ± 0.3 and 2.58 ± 0.2 for the inner ring and nucleus.

Measured $\frac{\rm [N\ II]_{6584}}{\rm H\alpha}$ and $\frac{\rm [S\ II]_{6716+6731}}{\rm H\alpha}$ ratios are used to determine metallicity following Nagao et al. (2006) and constrain the metallicity dependent $\alpha_{\rm CO}$. We find 12 + log(O/H) = 9.1 in the inner ring and $8.2 - 8.3$ for outer ring HII complexes with uncertainties of ≈ 0.15. Fig. 3 in Magdis et al. (2011) gives $\alpha_{\rm CO} = 25$ M$_\odot$ (K km s^{-1} pc^2)$^{-1}$ for the outer ring with a substantial spread reflecting the dispersion in individual measurements plus their uncertainties. Consequently, the correct $\alpha_{\rm CO}$ may lie between $3.7 - 90.0$ M$_\odot$ (K km s^{-1} pc^2)$^{-1}$. We adopt $\alpha_{\rm CO} = 25$ M$_\odot$ (K km s^{-1} pc^2)$^{-1}$ to derive $M_{\rm H_2}$, $\Sigma_{\rm H_2}$, and $f_{\rm mol}$ but give the full range implied by the $\alpha_{\rm CO}$ spread within parentheses.

3. Results and Discussion

3.1. CO Moment Maps

115 GHz line emission is directly detected only in the inner ring and nucleus (Fig. 1). We measure an integrated line flux of 12.86 ± 0.28 Jy km s^{-1} in agreement with single dish observations (Horellou et al. 1998), implying that ALMA recovers essentially all of the Cartwheel's CO emission. 72% originates in the inner ring where the clumpy gas distribution coincides with prominent dust lanes and luminous ($L_{\mathrm{H}\alpha} \approx 1 - 3 \times 10^{39}$ erg s^{-1}; $\mathrm{A}_{\mathrm{H}\alpha} = 1.9$) HII complexes. CO peaks are typically associated with Hα sources. Given the inner ring's metallicity and modest Σ_{SFR} we adopt a Galactic α_{CO} (3.68 M$_\odot$ (K km s^{-1} pc^2)$^{-1}$; Strong et al. 1988), giving a total $M_{\mathrm{H_2}}$ of $(1.94 \pm 0.04) \times 10^9$ M$_\odot$ and $\Sigma_{\mathrm{H_2}} = 8 - 148$ M$_\odot$ pc^{-2}. The remaining H$_2$, $(7.5 \pm 0.1) \times 10^8$ M$_\odot$ for a Galactic α_{CO}, originates in an unresolved nuclear source representing the galaxy's highest $\Sigma_{\mathrm{H_2}}$ (≥ 216 M$_\odot$ pc^{-2}). The inner ring and nucleus are both H$_2$-dominated ($f_{\mathrm{mol}} \approx 1$). CO emission is not evident anywhere else in the moment-0 map, implying $\Sigma_{\mathrm{H_2}} \lesssim 4$ M$_\odot$ pc^{-2} (3σ) for a Galactic α_{CO}.

The inner ring's CO velocity field (Fig. 2) displays ordered rotational motion along with streaming visible as kinks in the isovelocity contours. Although we expect the inner ring to be expanding we fit its radial velocity distribution with models of rotating circular rings both with and without expansion (V_{exp}; see HHR). An *expanding* circular ring ($i = 56.6°$) provides the best fit, giving $V_{\mathrm{sys}} = 9138.5 \pm 2.7$, $V_{\mathrm{circ}} = 170.3 \pm 5.2$ and $V_{\mathrm{exp}} = 68.9 \pm 4.9$ km s^{-1}. For the inner ring's 4.8 kpc radius an ≈ 70 Myr age is implied, or $\approx 1/6^{\mathrm{th}}$ the outer ring's.

3.2. CO Stacking Analysis

Stack averaging is used to pursue faint ^{12}CO(J=1-0) emission in the outer ring. We first divide it into three annular sections (I, II & III in Fig. 1) of approximately equal projected area using the HI and Hα images to define their width. Section II possesses both the Cartwheel's highest Σ_{HI} and $\approx 50\%$ of its total M_{HI}. CO spectra within a given section are coadded after being first shifted using the HI velocity at that position to place the 115 GHz line at the origin. The averaged spectra are then smoothed (24 km s^{-1} boxcar) and rebinned (8 km s^{-1}). We report the first detection of molecular gas in the Cartwheel's outer ring in section II (Fig. 3) and derive a mean CO intensity (I_{CO}) of 1.40 ± 0.16 mJy km s^{-1} arcsec^{-2} and a noticeably asymmetric profile ($\Delta V_{\mathrm{FWZI}} = 48$ km s^{-1}). For our adopted α_{CO} this represents $M_{\mathrm{H_2}} = (7.5 \pm 0.8) \times 10^8$ M$_\odot$ ($(0.8 - 25.3) \times 10^8$ M$_\odot$) and a mean $\Sigma_{\mathrm{H_2}}$ of 3.7 ± 0.4 M$_\odot$ pc^{-2} ($0.4 - 12.6$ M$_\odot$ pc^{-2}). In this section $M_{\mathrm{HI}} = 7.0 \times 10^9$ M$_\odot$, giving $f_{\mathrm{mol}} = 0.10 \pm 0.01$

$(0.01 - 0.27)$. CO emission is not detected from sections I or III after stacking ($I_{\rm CO} < 1.00$ and < 0.71 mJy km s^{-1} arcsec^{-2}, respectively), implying $M_{\rm H_2} \lesssim 3 \times 10^8$ M$_\odot$ $(0.4 - 9.3 \times 10^8$ M$_\odot$), $\Sigma_{\rm H_2} \lesssim 2 - 3$ M$_\odot$ pc^{-2} $(0.3 - 10.8$ M$_\odot$ pc$^{-2})$ and $f_{\rm mol} \lesssim 0.08$ $(0.01 - 0.28)$ on average over $\approx 2/3$ of the 45 kpc diameter outer ring.

To better define the H_2 distribution we subdivide the outer ring into eight annular sections ($a - h$ in Fig. 4) of ≈ 100 kpc^2 projected area using the same widths as before. Two sections of special interest due to their intense SF - the "northern arc" and "southern quadrant" ($\approx 80\%$ of $L_{\rm H\alpha}^{\rm total}$; Higdon 1995) - are represented by sections a and $d + e$ respectively. Stack averaging is done as before but with slightly increased smoothing (30 km s^{-1} boxcar) and rebinning (10 km s^{-1}). We detect ^{12}CO(J=1-0) only in b, c & d. All three sections are characterized by high $\Sigma_{\rm HI}$ but a wide range in $\Sigma_{\rm SFR}$. Emission is not detected in the northern arc and, unexpectedly, in only half of the southern quadrant (d but not e) despite similar $\Sigma_{\rm SFR}$ and $\Sigma_{\rm HI}$. We derive $I_{\rm CO}$ of (0.54 ± 0.11), (1.28 ± 0.24), and (1.60 ± 0.26) mJy km s^{-1} arcsec^{-2} for sections b, c and d, with $\Delta V_{\rm FWHM} = 20, 25$ and 39 km s^{-1}. CO in d is offset 20.4 ± 2.6 km s^{-1} from the origin and is responsible for the line asymmetry in section II. The other sections yield $\approx 0.80 - 1.56$ mJy km s^{-1} arcsec^{-2} (3σ) upper limits. For sections b, c & d we find $\Sigma_{\rm H_2}^{\text{"}b\text{"}} = 1.5$ M$_\odot$ pc^{-2} $(0.3 - 5.6$ M$_\odot$ pc$^{-2})$, $\Sigma_{\rm H_2}^{\text{"}c\text{"}} = 3.7$ M$_\odot$ pc^{-2} $(0.5 - 13.1$ M$_\odot$ pc$^{-2})$, and $\Sigma_{\rm H_2}^{\text{"}d\text{"}} = 4.6$ M$_\odot$ pc^{-2} $(0.7 - 16.3$ M$_\odot$ pc$^{-2})$. Given the sections' corresponding $\Sigma_{\rm HI}$ (28.8, 36.9 & 17.7 M$_\odot$ pc^{-2}) we derive $f_{\rm mol} = 0.05 - 0.21$. If we use the largest $\alpha_{\rm CO}$ consistent with the outer ring's metallicity (90 M$_\odot$ (K km s^{-1} pc^2)$^{-1}$; Magdis et al. 2011), $f_{\rm mol}$ only increases to $0.22 - 0.52$. Nowhere does the Cartwheel's starburst outer ring appear H_2-dominated.

3.3. H_2 Depletion Timescale and Star Formation Law

The Cartwheel's H_2 depletion timescale ($\tau_{\rm mol} = M_{\rm H_2}/SFR$) exhibits a wide range. In the nucleus and inner ring $\tau_{\rm mol} \approx 5 - 6$ Gyr, similar to values derived in local spiral disks (e.g., B08). Much smaller values characterize the outer ring particularly where $\Sigma_{\rm SFR}$ is high: $\tau_{\rm mol} = 52$ and < 50 Myr in d & e, which is shorter than the outer ring's rotational period (≈ 0.5 Gyr; Higdon 1996) and comparable to the main-sequence lifetime of a B-star. $\tau_{\rm mol}$ is larger in b and c (640 & 189 Myr) and similar to disk averaged $\tau_{\rm mol}$ for starburst galaxies (e.g., Kennicutt 1998). Elsewhere in the outer ring $\tau_{\rm mol} < 160 - 530$ Myr (3σ).

We show the Cartwheel's molecular and atomic SF laws in Fig. 5 and compare them to those derived for nearby galaxies on comparable spatial scales where $\Sigma_{\rm SFR}$ is also estimated using H$\alpha + 24$ μm emission. The Cartwheel's two rings present very different distributions: the 11 inner ring HII complexes and nucleus together are consistent with M51's spatially-

resolved H_2 SF law ($\Sigma_{SFR} \propto \Sigma_{H_2}^{1.37}$; K07); SF in the outer ring appears to be independent of Σ_{H_2} in a manner similar to AM0644-741's ring (Fig. 14 in HHR). This is in marked contrast to the azimuthally averaged molecular SF law derived for the CO-bright disks of the HERACLES survey (Leroy et al. 2009a, L13) where $\Sigma_{SFR} \propto \Sigma_{H_2}$. The HI-dominated outer-disks of spirals are characterized by reduced metallicity and dust/gas ratios and should therefore more closely resemble conditions in the Cartwheel's outer ring. Fig. 5 shows that the averaged outer-disk ($> 0.5\ r_{25}$) molecular SF law for the HERACLES sample still shows a tight linear relation between Σ_{SFR} and Σ_{H_2} (S11), which is again quite unlike the outer ring's SF law. One might argue that points b, c and d define a steep power law relation ($\Sigma_{SFR} \propto \Sigma_{H_2}^{3.5}$). Any such correlation, however, is greatly weakened by the five H_2 upper-limits and the wide range in Σ_{H_2} allowed by the α_{CO} dispersion, which together comprise a large systematic uncertainty.

HI in the Cartwheel's outer ring reaches $\Sigma_{HI} = 19 - 65\ M_\odot\ pc^{-2}$ and, like H_2, appears independent of Σ_{SFR} (Fig. 5). This resembles the HI "saturation" observed in spiral galaxies ($\approx 8\ M_\odot\ pc^{-2}$; K07, B08, S11), though with significantly higher Σ_{HI}. Because f_{mol} is so small, the outer ring's combined HI+H_2 SF law is, in effect, the HI SF law (Fig. 5). For local spirals the exact opposite opposite is true. A vertical line can be drawn through all but one point (within the uncertainties) for the Cartwheel's outer ring, leading to the unusual result that SF appears independent of the local neutral gas surface density in any form: atomic, molecular or combined.

Normal SF laws break down on small spatial scales and after $\gtrsim 30$ Myr for individual SF regions (e.g., S10). However, given the $\approx 36\ kpc^2$ area of regions $a - h$ and the evidence for continuous SF (§1) as the rings propagate, other factors must be responsible for the Cartwheel's (and AM0644-741's) peculiar SF law. It is moreover extremely unlikely that the entire SF region populations of both outer rings happen to be in the same brief (≈ 20 Myr) CO-faint/Hα-luminous phase.

Consumption of the ring's ISM due to high Σ_{SFR} could deflect points to the left in Fig. 5. Indeed, Higdon (1996) noted a significant decrease in Σ_{HI} across sections d & e, which is visible in Fig. 4. However the observed Σ_{SFR} would require ≈ 3 Gyr - roughly 7-times the ring's estimated age - to shift points d and e to their observed positions starting from any of the spiral galaxy SF laws shown. While gas depletion effects may be at work they cannot be entirely responsible for the observed SF law unless Σ_{SFR} was much higher in the past.

3.4. The Outer Ring's ISM

CO emission from the Cartwheel's outer ring indicates an extremely H_2 poor ISM even after accounting for its sub-solar metallicity. In trying to understand this situation we discount the possibility that we are viewing the Cartwheel (and AM0644-741) just as their molecular reservoirs have been exhausted, since both rings' high $\Sigma_{\rm HI}$ favors the rapid conversion of HI to H_2. It may be the case that conditions in the starburst ring lead to enhanced destruction of H_2 so that even a metallicity-appropriate $\alpha_{\rm CO}$ reveals little molecular gas. This however leaves the question of how SF is triggered so efficiently in the remaining H_2. Alternately, the starburst rings may act to make CO an unreliable proxy for H_2. The ability of CO to trace H_2 in a molecular cloud (MC) depends sensitively on the cloud's net visual extinction, $\overline{A}_{\rm V}$, which is proportional to the product of its metallicity and H_2 column density ($N_{\rm H_2}$) (e.g., Wolfire, Hollenbach & McKee 2010; Clark & Glover 2015; Lee et al. 2015). Small or low-$n_{\rm H}$ (or both) MCs in active star forming regions may inadequately shield the fragile CO molecule and as a result become extremely CO-faint. Reduced metallicity substantially compounds this effect. We propose that the ISM's long confinement in the starburst rings of these systems can result in a state characterized by smaller MCs and a diffuse H_2 component due to the accumulated damage from embedded OB stars and SNe (HHR). This helps explain the extremely low average $n_{\rm H}$ ($1-5$ cm^{-3}) we derive for AM0644-741's starburst quadrant. If this characterizes the overall state of the ISM then low-$N_{\rm H_2}$ MCs may dominate high $\Sigma_{\rm SFR}$ regions, resulting in a CO-faint molecular ISM and low inferred $M_{\rm H_2}$. A further dependence on metallicity and local $\Sigma_{\rm SFR}$ would be expected to produce a peculiar SF law like that in Fig. 5. Conversely, the inner ring's ≈normal $\Sigma_{\rm H_2}$, $f_{\rm mol}$, $\tau_{\rm mol}$ and SF law would be a consequence of its lower $\Sigma_{\rm SFR}$ and age (70 vs. 440 Myr): the inner ring's ISM has yet to reach the outer ring's state.

These possibilities can be further tested observationally. Dense ($n > 10^4$ cm^{-3}) gas in cloud cores should be better protected from the destructive effects of massive stars and is, moreover, the component directly connected with SF (Solomon et al. 1992; Gao & Solomon 2004). Observations of the Cartwheel and AM0644-741 using HCN or HCO+ rotational transitions may uncover ≈normal SF laws. Infrared/submillimeter dust emission would additionally provide reliable estimates of H_2 in the rings independent of CO (e.g., Leroy et al. 2009b). Our analysis further suggests that high $\Sigma_{\rm SFR}$ and long residence time are both required to reach the peculiar ISM state we infer in starburst rings. Observations of *young* ring galaxies (i.e., age $\lesssim 100$ Myr) would in this case be expected to show more normal $f_{\rm mol}$ and SF laws. Preliminary support for this is suggested by the global $f_{\rm mol}$ (0.40) of the young (*age* ≈ 35 Myr) ring galaxy Arp 147. State of the art ring galaxy models incorporating a multi-phase ISM and the effects of massive stars and SNe will also help place these ideas on a firmer physical basis.

4. Conclusions

Both of the Cartwheel's rings are gas rich, expanding and forming stars, though with large differences in their relative SFR, $\Sigma_{\rm SFR}$ and ages. They appear dominated by different ISM phases: molecular in the inner and atomic in the outer. Even with a metallicity appropriate $\alpha_{\rm CO}$ the outer ring's H_2 content appears strikingly low for its star formation activity, which leads directly to its unusually low $\tau_{\rm mol}$ and peculiar SF law. By contrast the inner ring appears normal. Similar results were found in AM0644-741's 42 kpc diameter starburst ring, leading us to reject the possibility that we are observing both ring galaxies just as their H_2 reservoirs are consumed or when their SF regions simultaneously attain a brief CO-faint/Hα-luminous phase. Either highly efficient SF occurs in a H_2-poor ISM in the rings of these systems or rotational transitions of ^{12}CO do not accurately trace H_2. Our observations are consistent with the second explanation if the ISM of both starburst rings possess abundant small and/or low-$N_{\rm H_2}$ MCs that inadequately shield CO molecules. This is a direct consequence of the ISM's long residence in the outer rings and is very likely compounded by sub-solar metallicity in addition to (limited) gas depletion effects. If so, the outer ring's $M_{\rm H_2}$ and $\Sigma_{\rm H_2}$ may be substantially greater than that inferred by CO. We expect such a state to characterize large and robustly star forming ring galaxies and possibly starburst nuclear rings associated with gravitational resonances. The large departures from a standard SF law we derive in the outer rings of the Cartwheel and AM0644-741 represent interesting puzzles that a comprehensive theory of star formation should be able to address.

This Letter makes use of ALMA dataset ALMA#2012.1.00720.S. ALMA is a partnership of ESO (representing its member states), NSF (USA), and NINS (Japan), together with NRC (Canada) and NSC and ASIAA (Taiwan), in cooperation with the Republic of Chile. The Joint ALMA Observatory is operated by ESO, AUI/NRAO, and NAOJ. Based on observations collected at the European Organization for Astronomical Research in the Southern Hemisphere under ESO programs 66.B-0666(A) and 66.B-0666(B). The National Radio Astronomy Observatory is a facility of the National Science Foundation operated under cooperative agreement by Associated Universities, Inc. This work is based in part on observations made with the *Spitzer Space Telescope*, which is operated by the Jet Propulsion Laboratory, California Institute of Technology under a contract with NASA. The authors thank K. Sheth for the initial reduction of the ALMA data, G. Cecil for his role in the spectroscopic observations, and the Paranal observatory staff for the VLT service observations. We thank an anonymous referee for constructive comments.

REFERENCES

Appleton, P. N., Struck-Marcell, C., Bransford, M. A., Charmandaris, V., Marston, A. et al. 1996, in I.A.U. Symp. 171, New Light on Galaxy Evolution, ed. R. Bender & R. L. Davies (Kluwer, Dordrecht), 337

Bigiel, F., Leroy, A., Walter, F., Brinks, E., de Blok, W. et al., 2008, AJ, 136, 2846 (B08)

Clark, P. C., & Glover, S. C. 2015, MNRAS, 452, 2057

Fosbury, R. A. E., & Hawarden, T. G. 1977, MNRAS, 178, 473

Gao, Y. & Solomon, P. 2004, ApJ, 606, 271

Higdon, J. L. 1995, ApJ, 455, 524

Higdon, J. L. 1996, ApJ, 467, 241

Higdon, J. L., Higdon, S. J. U., & Rand, R. J. 2011, ApJ, 739, 97 (HHR)

Horellou, C., Charmandarys, V., Combes, F., et al. 1998, A&A, 340, 51

Horellou, C., Casoli, F., Combes, F. et al., 1995, A&A, 298, 743

Jogee, S., Miller, S. H., Penner, K., et al. 2009, ApJ, 697, 1971

Kennicutt, R. C. 1998, ApJ, 498, 541

Kennicutt, R. C., Calzetti, D., Walter, F., et al. 2007, ApJ, 671, 333 (K07)

Lee, C., Leroy, A. K., Schnee, S., et al. 2015, MNRAS, 450, 2708

Leroy, A. K., Walter, F., Bigiel, F. et al. 2009, AJ, 137, 4670

Leroy, A. K., Bolatto, A., Bot, C., et al. 2009, ApJ, 702, 352

Leroy, A., Walter, F., Sandstrom, K., Schruba, A., Munoz-Mateos, J. et al. 2013, AJ, 146, 19 (L13)

Lynds, R. & Toomre, A. 1977, ApJ, 209, 382

Magdis, G. E., Daddi, E., Elbaz, D., Sargent, M., Dickinson, M. et al., 2011, ApJ, 740, 15

Mapelli, M., Moore, B., Ripamonti, E., et al. 2008, MNRAS, 383, 1223

Mapelli, M., & Mayer, L. 2012, MNRAS, 420, 1158

Marcum, P. M., Appleton, P., & Higdon, J. L. 1993, ApJ, 399, 57

McMullin, J. P., Waters, B., Schiebel, D., Young, W., & Golap, K. 2007, in ASP Conf. Ser. 376, Astronomical Data Analysis Software and Systems XVI, ed. R. A. Shaw, F. Hill, & D. J. Bell (San Francisco, CA: ASP), 127

Mihos, J. C., & Hernquist, L. 1994, ApJ, 437, 611

Nagao, T., Maiolino, R., & Marconi, A. 2006, A&A, 459, 85

Romano, R., Mayya, Y., & Vorobyov, E. 2008, AJ, 136, 1259

Schruba, A., Leroy, A., Walter, F., Bigiel, F., Brinks, E. et al. 2011, AJ, 142, 37 (S11)

Smail, I., Ivison, R. J., & Blain, A. W., 1997, ApJ, 490, L5

Solomon, P. M., Downes, D., & Radford, S. J., 1992, ApJ, 387, 55

Solomon, P. M., & Vanden Bout, P. A. 2005, ARAA, 43, 677

Strong, A. W., Bloemen, J., Dame, T., et al. 1988, A&A, 207, 1

Struck, C. J., & Higdon, J. L. 1993, ApJ, 411, 108

Tacconi, L. J., Genzel, R., Smail, I., et al. 2008, ApJ, 680, 246

White, S. D., & Rees, M. J. 1978, MNRAS, 183, 341

Wolfire, M. G., Hollenbach, D., & McKee, C. F. 2010, ApJ, 716, 1191

This preprint was prepared with the AAS LaTeX macros v5.2.

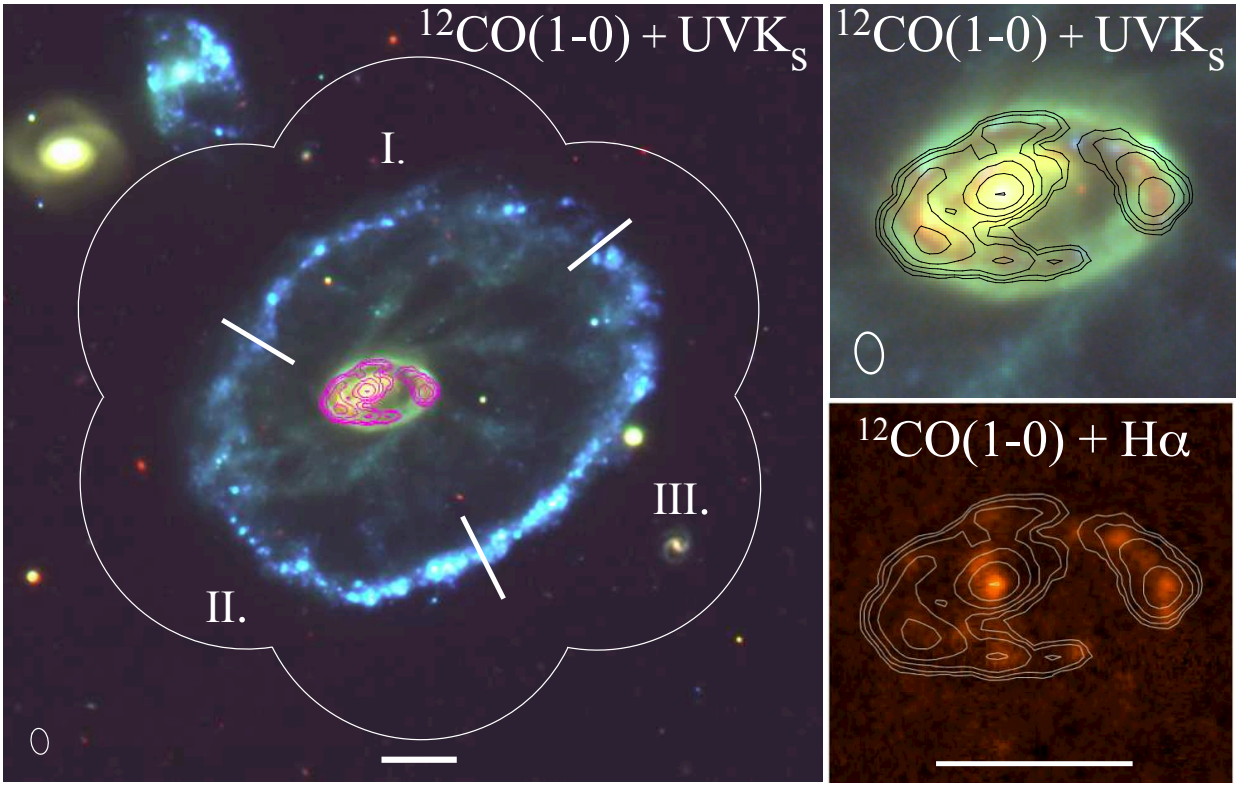

Fig. 1.— Molecular gas in the Cartwheel. (left) *natural*-weighted ^{12}CO(J=1-0) emission (moment-0) contoured on a VLT UVKs three-color image with six of the seven-position mosaic primary beams (53″ FWHM) outlined. Contours correspond to Σ_{H_2} = 6.8, 15.9, 37.3, 87.2 & 204.0 $M_\odot$ pc^{-2} for a Galactic α_{CO} and include helium. Only the inner ring and nucleus are directly detected. The synthesized beam (2.43″ × 1.50″) is shown at bottom-left. (top-right) A close-up of the inner ring's CO emission, including Hα emission (bottom-right). Both scale-bars are 10″ (6.1 kpc).

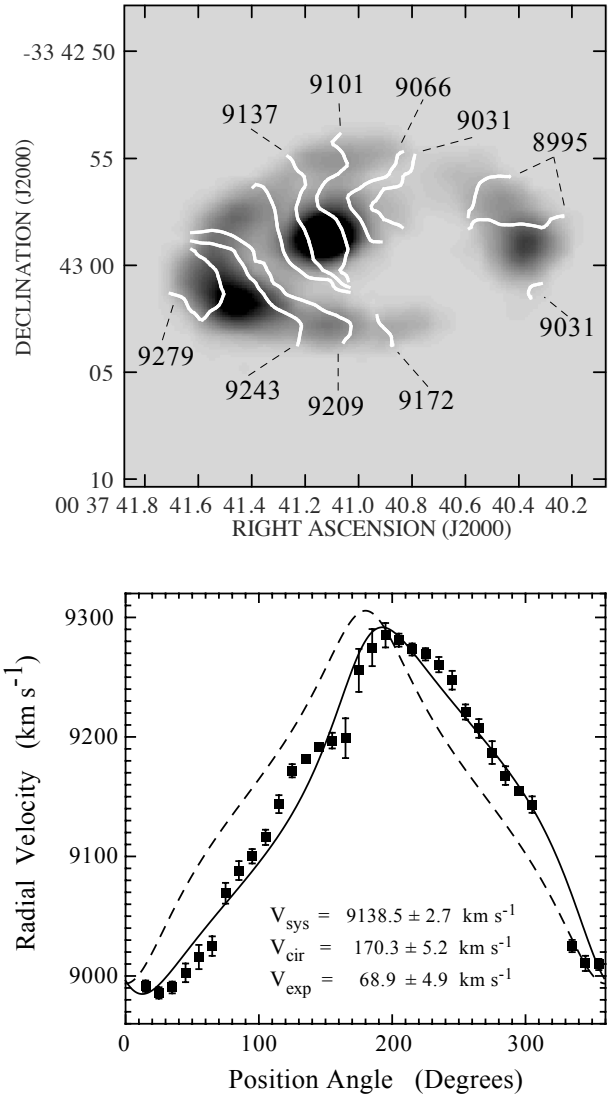

Fig. 2.— The inner ring's CO kinematics. (top) Isovelocity contours (optical/heliocentric) from the moment-1 map shown plotted on the moment-0 greyscale image. (bottom) The inner ring's radial velocity-position angle diagram showing least-square fits for inclined rotating circular rings with (solid) and without (dashed) expansion.

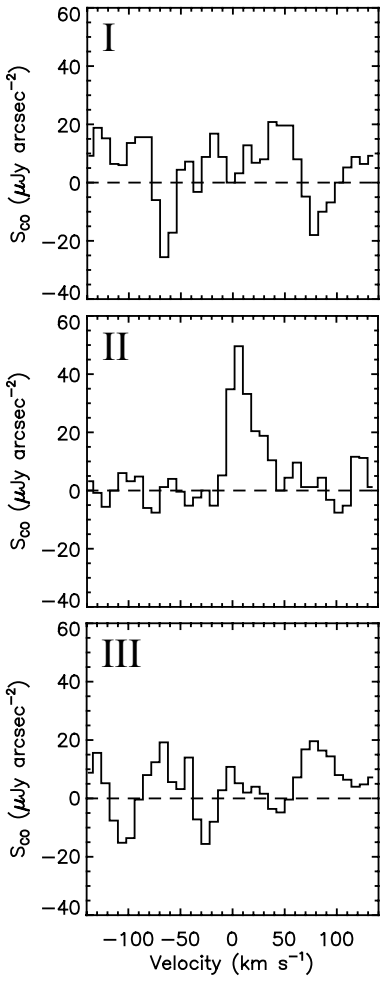

Fig. 3.— Stack averaged ^{12}CO(J=1-0) spectra for sections I, II and III of the Cartwheel's outer ring as defined in Fig. 1. Molecular gas is detected only in section II.

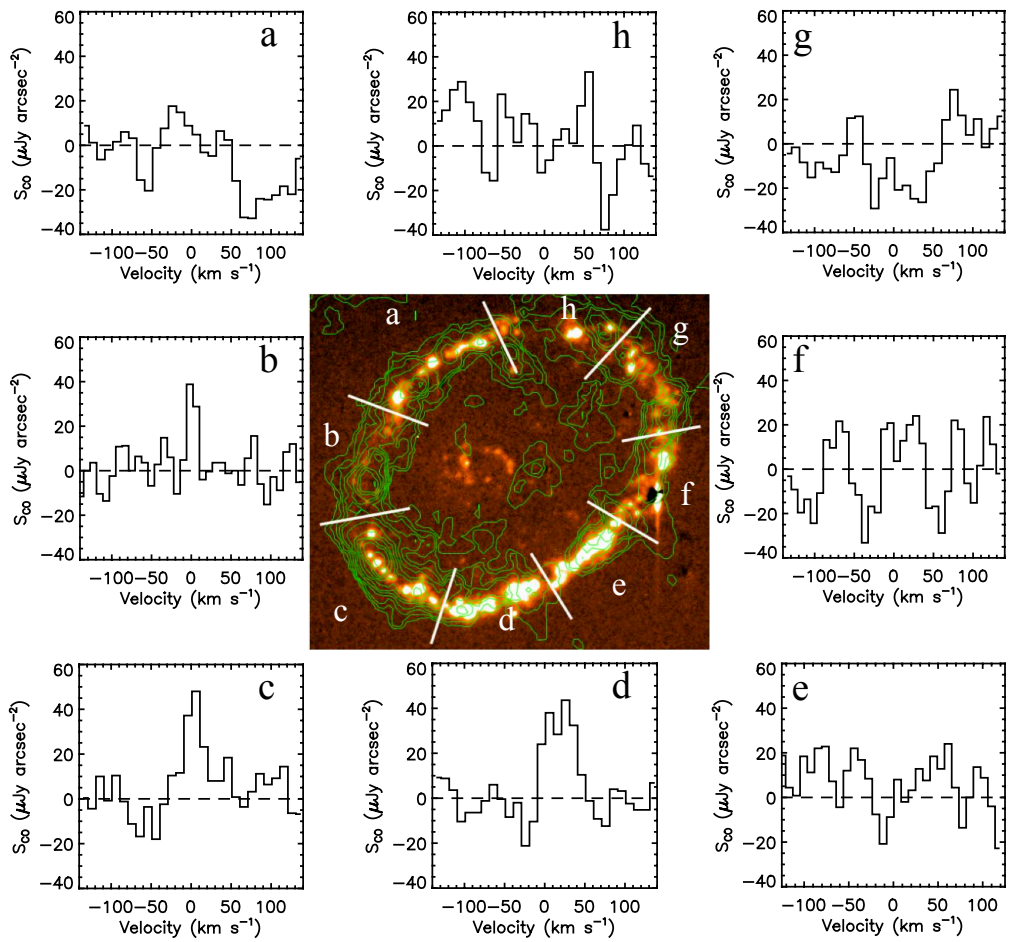

Fig. 4.— Stack averaged ^{12}CO(J=1-0) spectra for the eight sections of the Cartwheel's outer ring as defined for the Hα image (color in the electronic version) at center. Molecular gas is detected only at $b-d$, which corresponds to II in Fig. 1. Contours represent $\Sigma_{\rm HI}$ = 2.7, 4.1, 6.3, 9.4, 14.3, 21.5 & 32.6 M$_\odot$ pc^{-2} and include helium.(Higdon 1996).

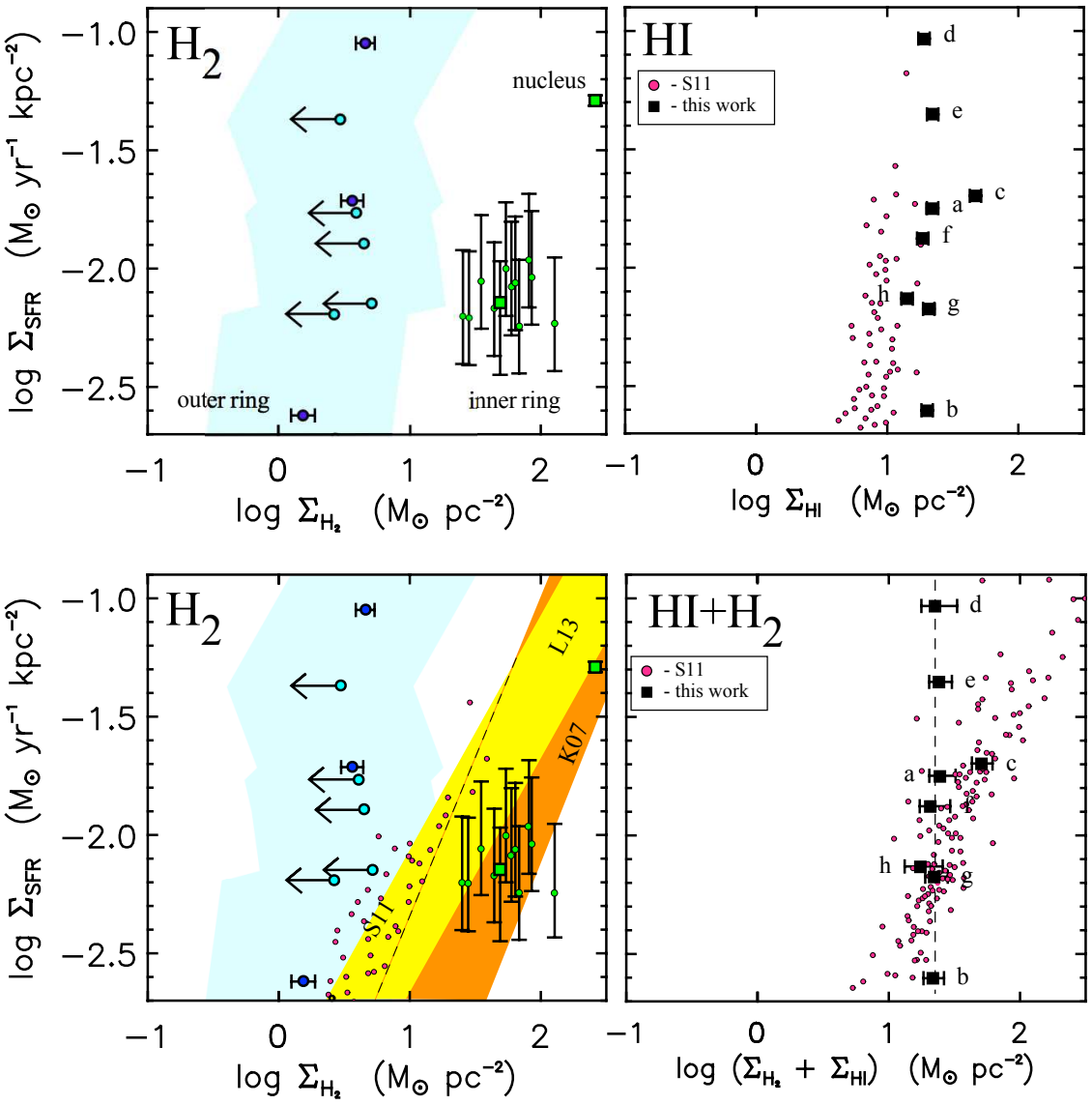

Fig. 5.— The Cartwheel's SF law. (top-left) Derived H_2 SF law for the outer and inner rings. The nucleus and averaged inner ring are represented by squares. The shaded area indicates the allowed Σ_{H_2} given α_{CO}'s dispersion in Magdis et al. (2011). (bottom-left) The Cartwheel's molecular SF law compared with M51's spatially-resolved molecular SF law (K07), the azimuthally averaged SF law for the HERACLES sample of local spirals and irregulars (L13), and their outer ($> 0.5\ r_{25}$) HI-dominated disks only (S11). The latter assumes a Galactic α_{CO}. (top-right) The Cartwheel's HI SF law compared to the HI-dominated outer disks in the HERACLES survey (S11). (bottom-right) The outer ring's total gas SF law. Σ_{SFR} appears independent of Σ_{HI+H_2}. The corresponding total SF law derived with the HERACLES sample is also shown.